JOURNAL OF APPLIED ELECTROCHEMISTRY **28** (1998) 835–841

Oxygen evolution on electrodeposited cobalt oxides

E. B. CASTRO*, C. A. GERVASI‡, J. R. VILCHE

Instituto de Investigaciones Fisicoquímicas Teóricas y Aplicadas (INIFTA), Suc. 4, C.C. 16, (1900) La Plata, Argentina

Received 7 April 1997; revised 25 July 1997

This paper concerns the preparation of cobalt oxides through anodic deposition from $Co(NO_3)_2$ aqueous solutions on different substrates. The electroformed oxide films exhibit good chemical stability and lower oxygen overvoltages, irrespective of the substrate material. Electrocatalytic properties are investigated through polarisation curves and impedance measurements, while the active surface area is estimated by cyclic voltammetry. Experimental data are analysed in terms of a possible reaction mechanism.

Keywords: *anodic catalysts*, *cobalt oxides*, *oxygen evolution reaction*

1. Introduction

The importance of transition metallic oxide electrodes as catalysts is well documented. In particular, the electrocatalysis of oxygen evolution on these electrodes has been a topic of great interest, since oxygen evolution is an unavoidable side reaction in many anodic processes and it is the most common anodic reaction coupled with most of the cathodic processes occurring in aqueous solutions such as water electrolysis and metal electrowinning. Optimization of the electrolysis parameters starts with the appropriate selection of electrode materials. Different preparation processes often lead to materials exhibiting widely differing electrocatalytic behaviour.

Oxides of the spinel type have received most attention. Cobaltites (MCo_2O_4 with M = Co, Zn, Ni, Cu etc.) are among those oxides on which work is in progress [1–4]. Due to their excellent electrocatalytic properties and enhanced surface active area, cobaltites are efficient electrocatalysts for oxygen evolution in alkaline solutions [1]. Generally, a binary spinel oxide, $Ni_xCo_{3-x}O_4$, with a surface Co/Ni ratio of two, has the highest electrocatalytic activity for oxygen evolution [3]. Oxide films are usually formed by thermal decomposition, spray pyrolysis and sputtering. One main drawback in the preparation of deposited catalysts is that in the course of the thermal treatment the oxidation of the substrate (mainly Ti), or a reduction of the active surface, cause the anode performance to deteriorate.

In this work we investigate oxygen evolution on electrodeposited Co oxide films on different substrates, as a means of preparing thin film electrocatalysts. Some of the substrate materials were selected since they exhibit high activation overpotentials for oxygen evolution and are not expected to contribute directly in any significant way to the electrocatalytic behaviour of the overlaying films.

2. Experimental details

2.1. *Solutions*

Solution A: 1 M aqueous NaOH, (pH 14).

Solution B: 0.05 M $Co(NO_3)_2 6H_2O$ + 0.5 M $NaNO_3$ (pH ~ 4).

All reagents were Merck, *pro analysi*, and were used without further treatment. All measurements and electrodeposition were performed in three-compartment cells (capacity 250 ml) under nitrogen gas saturation. The rotation speed, ω, was 2000 rpm in all experiments, and the working temperature was 25 °C.

2.2. *Electrodes*

Cobalt oxide films were electrodeposited, on rotating disc electrodes of platinum (area 0.07 cm^2), vitreous carbon (0.1 cm^2), iron (0.1 cm^2) and nickel (0.1 cm^2) ('Specpure' Johnson Matthey). Prior to deposition the rotating disc electrodes were polished with 1 and 0.3 μm alumina and carefully rinsed with milli-Q water. A high area Pt foil, was used as auxilliary electrode. Potentials were measured against a saturated calomel electrode (SCE) in solution B and against a Hg/HgO/1M OH^- electrode in solution A. All potentials in the text are referred to the Hg/HgO reference electrode in the same solution.

2.3. *Electrochemical measurements*

Cyclic voltammetry and potentiostatic polarisation were used for the electrodeposition as well as for the characterization of the electrochemical behaviour of the oxide films. Electrochemical impedance spectroscopy was used to study the kinetics of the oxygen

*Author to whom correspondence should be submitted.
‡CIC researcher.

0021-891X

evolution reaction (OER). Steady-state potentiostatic polarisation and cyclic voltammetric measurements were performed with a EG&G M273 potentiostat combined with EG&G M270 software on an IBM compatible PC. Electrochemical impedance measurements were performed using the above mentioned potentiostat and a Schlumberger SI 1255 HF frequency response analyser. The data sets obtained from impedance measurements were analyzed by means of a nonlinear least squares fit (NLLS) routine employing a modification of the Levemberg–Marquardt method [5].

3. Results

3.1. *Electrodeposition methods*

Cobalt oxides were electrodeposited on Ni, Pt, Fe and vitreous carbon disc electrodes. Electrodeposits were prepared by the following two methods.

3.1.1. Potentiostatic electrodeposition (electrodes I). Disc electrodes of the different substrates were polarised at $E = 0.5$ V (vs Hg/HgO ss), in 200 ml of solution B. Immediately after the application of the potentiostatic signal, 10 ml of sol A were added. A blue precipitate was formed, (probably $Co(OH)_2$[7]), which remained in suspension due to electrode rotation. The electrode was held at $E = 0.5$ V and $\omega = 2000$ rpm for 60 min. After electrodeposition the electrode was rinsed with milli-Q water. The electrode surface was covered in all cases by a black film.

3.1.2. Potentiodynamic electrodeposition (electrodes II). Nickel disc electrodes were subjected to repetitive triangular potential scans (RTPS), in solution A (1 M NaOH, 200 ml) + 10 ml of sol B, between $E_{sc} = -0.1$ V and $E_{sa} = 0.7$ V, at $v = 0.05\ \mathrm{V\,s^{-1}}$ for 60 min, $\omega = 2000$ rpm. Prior to the application of the RTPS the electrode was polarized at $E = -1.2$ V for 5 min, in sol A, to reduce air formed films. Immediately after the RTPS was applied, sol B was added. As described above a blue precipitate was formed. After electrodeposition the electrode was rinsed with milli-Q water. The electrode surface was covered by a bright golden film.

3.2. *Characterization of the Co oxide electrodeposits*

3.2.1. Voltammetric characterization. The electrochemical behaviour of the electrodeposits prepared by both methods outlined in Section 3.1 was analysed in 1 M NaOH (sol A).

Electrodes I :
Figures 1 and 2 (curves (a)) show cyclic voltammograms corresponding to electrodes I on Ni and vitreous C, respectively. Voltammograms obtained with clean substrates in sol A are included (curves (b)). The voltammetric profiles, corresponding to a potential scan between $E_{sc} = -0.1$ and $E_{sa} = 0.7$ V exhibit two very reversible couples, at 0.2 and 0.55 V. These voltammograms are very similar to cyclic voltammograms corresponding to Co_3O_4 oxides with spinel structure prepared by spraying or sputtering on different substrates [6, 8, 9], exhibiting reversible couples with current peaks at identical potentials. These couples may be assigned to the Co(II)/Co(III) and Co(III)/Co(IV) redox processes [9]. Thermodynamic redox potentials corresponding to Co_3O_4/CoOOH and CoOOH/CoO_2 are $E = 0.222$ and $E = 0.562$ V vs (Hg/HgO 1M OH^-), respectively.

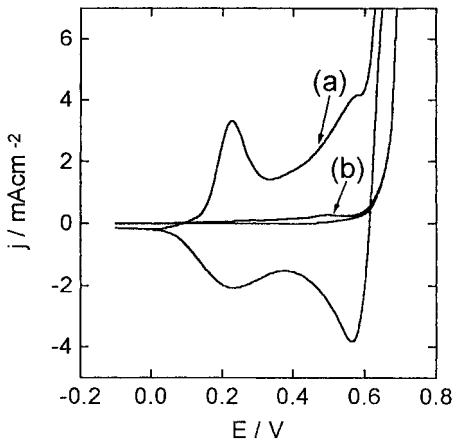

Fig. 1. Curve (a), cyclic voltammograms corresponding to electrodes I on a Ni substrate (1st cycle and stabilized profile). Curve (b), clean Ni electrode (1st cycle), in NaOH 1 M. $v = 0.01\ \mathrm{V\,s^{-1}}$.

Two facts are evident from the voltammetric response. Firstly, any electrochemical process occuring at the substrate is completely masked by redox processes corresponding to the electrodeposited Co oxide, as voltammograms corresponding to different substrates exhibit identical features. This does not necessarily mean that no electrochemical process takes place at the substrate. Processes like oxide formation, space charge layer charging and metal dissolution may take place, although their contribution to the total voltammetric current may be disregarded. Secondly, the current related to the OER is noticeably enhanced.

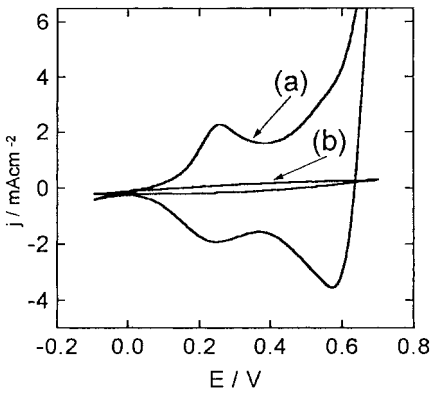

Fig. 2. Cyclic voltammograms corresponding to electrodes I on a vitreous C substrate (curve (a), 1st cycle and stabilized profile) and to clean vitreous C electrode (curve (b), 1st cycle), in NaOH 1 M. $v = 0.01\ \mathrm{V\,s^{-1}}$.

The voltammetric cathodic charge is close to 10 mC. Considering that the charge corresponding to the electroreduction of the Co species to the oxidation state +2 is approximately 0.5 mC cm^{-2} [3], an interfacial area of 20 cm^2 can be estimated. This estimation is valid if the surface/bulk volume ratio for the electrodeposit is very high, which means that the major contribution to the total voltammetric current corresponds to processes taking place at the film/solution interface.

Electrodes II:
Figure 3 shows voltammograms corresponding to electrodes II, (curve (a), 1st cycle), voltammograms corresponding to clean Ni (for $\tau = 5$ and 60 min) are included (curves (b_1) and (b_2)). The voltammetric profile exhibits current maxima at more cathodic potentials than those corresponding to the Ni(II)/Ni(III) transition on clean Ni [10]. The electroreduction voltammetric charge is approximately 0.4 mC; this value corresponds to an estimated interfacial area of 0.8 cm^2, or to a roughness factor of 8. The anodic current related to the OER is also enhanced. The voltammetric profile of the electrodeposit is very similar to voltammograms corresponding to $Ni_xCo_{3-x}O_4$ (prepared by different methods) in 1 M OH^- [3, 6].

3.2.2. Electrochemical impedance spectroscopy characterization. Cobalt oxide electrodeposits, prepared by the methods described in Section 3.1, were subjected to impedance measurements in 1 M NaOH.

Electrodes I:
The impedance spectra presented in the present work were recorded at $E = 0.55$ V, which corresponds to the potential of the second reversible couple in Figs 1 and 2.

Figure 4, shows Nyquist plots, measured at $E = 0.55$ V, corresponding to electrodes I on Fe, Ni, Pt and vitreous C. All diagrams exhibit identical features; only small changes in values of IZI can be detected, specially for Pt substrate. Impedance spectra exhibit a capacitive behaviour in practically all the frequency range (0.1 Hz $\leq f \leq 1 \times 10^5$ Hz). A value of $C_{pc} \approx 2 \times 10^{-1}$ F cm^{-2}, for Fe and Ni substrates and $C_{pc} \approx 2 \times 10^{-2}$, for Pt substrate, can be estimated from the low frequency data, where C_{pc} corresponds to a pseudo-capacitance related to the reversible surface process occuring at $E = 0.55$ V. At this potential the impedance response is dominated by the redox process taking place at the Co oxide/electrolyte interface, probably the oxidation of Co(III) surface states to Co(IV).

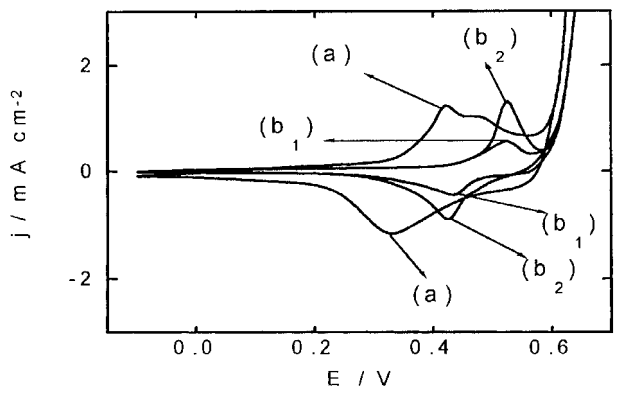

Fig. 3. Voltammetric response of electrodes II (curve (a), 1st cycle), in NaOH 1 M. Curves (b_1) and (b_2) correspond to clean Ni at different RTPS times (b_1) = 5 min, 2nd cycle, (b_2) = 60 min, 22th cycle), $v = 0.05$ V s^{-1}

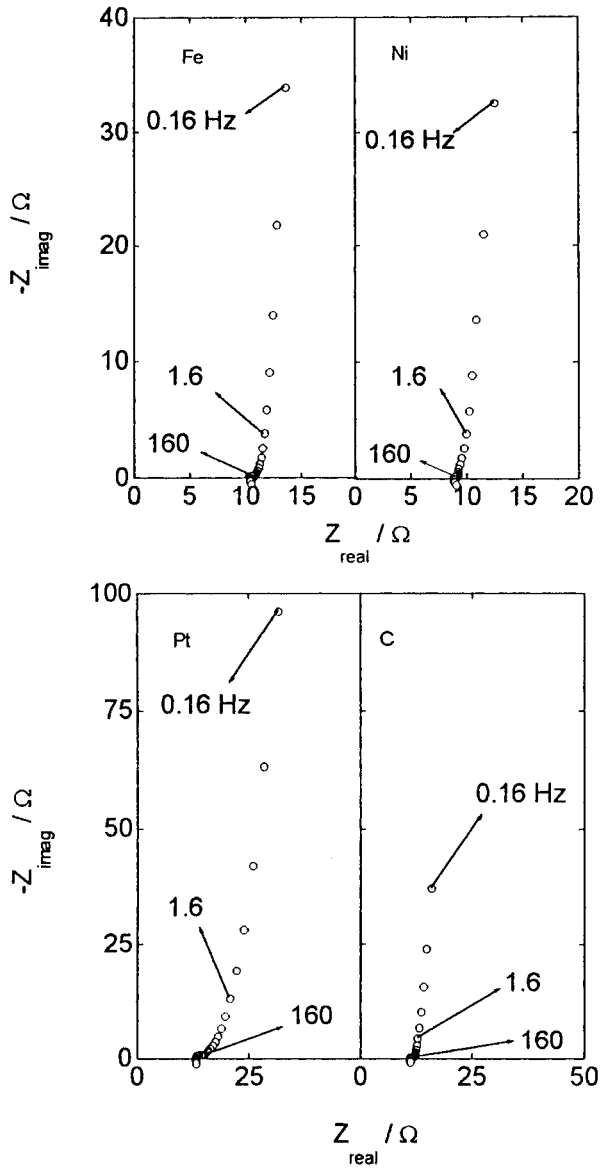

Fig. 4. Nyquist plots measured at $E = 0.55$ V, in 1 M NaOH, 0.15 Hz $< f < 10^5$ Hz, corresponding to electrodes I prepared on Fe, Ni, Pt and vitreous C.

Electrodes II:
In Fig. 5 a Nyquist diagram corresponding to electrode II at $E = 0.54$ V is depicted. In contrast with impedance spectra of Fig. 4, a finite resistance value can be determined from the system impedance when $f \rightarrow 0$ Hz, this fact being a probable indication of the onset of the OER.

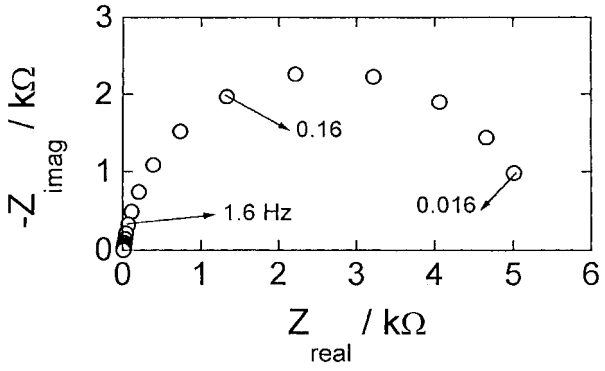

Fig. 5. Nyquist diagram measured at $E = 0.54$ V, in 1 M NaOH, corresponding to electrodes II.

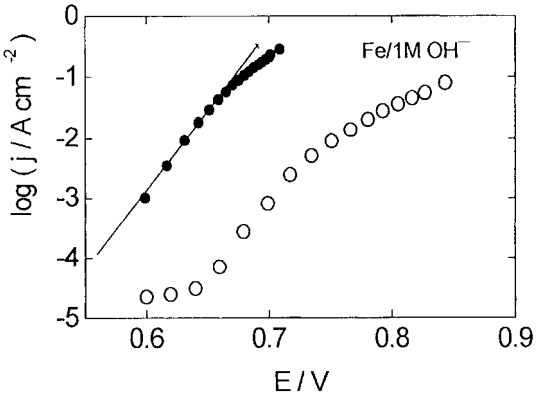

Fig. 7. Polarization plots for oxygen evolution in 1 M NaOH, 25 °C, corresponding to (●) electrodes I on Fe and (○) clean Fe.

3.3. *Oxygen evolution reaction (OER)*

3.3.1. Potentiostatic measurements. Electrodes I and II showed enhanced OER currents with respect to the corresponding bare substrates. Steady state polarization curves were recorded in 1 M NaOH, 25 °C. The OER current, at a given potential, attained steady-state values in approximately 10 min, exhibiting long-term stability at the operational potential. Cobalt electrodeposits also showed good stability in air, the OER current after 24 h of exposure to air or to 1 M NaOH, being only 10% smaller.

Figures 6 and 7 show polarization plots corresponding to electrodes I on Pt and Fe; corrections due to the electrolyte resistance have been taken into account. The current density is calculated using the geometric area. Polarization plots corresponding to the clean substrates in 1 M NaOH, are included. At low overpotentials an approximate value for the Tafel slope, $b_t = 40\,\text{mV dec}^{-1}$, is estimated. At higher overpotentials an increase in b_t is evident. In this potential range a profuse evolution of oxygen bubbles was observed, so a change in b_t cannot be readily assigned to a change in the rate determining step (r.d.s.) of the reaction pathway.

Figure 8 includes polarisation plots corresponding to electrodes II and electrodes I on Ni, together with steady-state data corresponding to clean Ni in 1 M NaOH. In the low overpotential range a better performance may be assigned to electrode II as compared with electrode I, taking into account the voltammetric estimation of real surface areas previously reported. Tafel slopes close to $b_t = 40\,\text{mV dec}^{-1}$ are estimated at low overpotentials.

The OER current densities, evaluated in terms of geometric area, in 1 M NaOH and 25 °C, corresponding to these electrodeposited Co oxides, are higher than those reported for Co_3O_4 and $NiCo_2O_4$ films obtained by spray pyrolysis [14], Ru–Ir binary oxides deposited on Ti [15] and Ti/SnO_2 + $CuCo_2O_4$ [16], having an apparent reactivity similar to Ti/RuO_2 + TiO_2 [16]. These electrodeposits also exhibit higher OER current densities than NiO(OH) and Co(III)-oxide electrodeposited on Pt and graphite electrodes from sodium acetate aqueous solutions containing either $NiSO_4$ or $Co(OAc)_2$ [22].

3.3.2. Electrochemical impedance spectroscopy. Impedance data measured at $E = 0.6$ and 0.7 V, corresponding to electrodes I on Pt and Fe, are shown in Figs 9 and 10, respectively. Nyquist plots corresponding to Ni substrate exhibit similar features as compared with Pt, only one slightly distorted capacitive loop being observed. Nyquist plots corre-

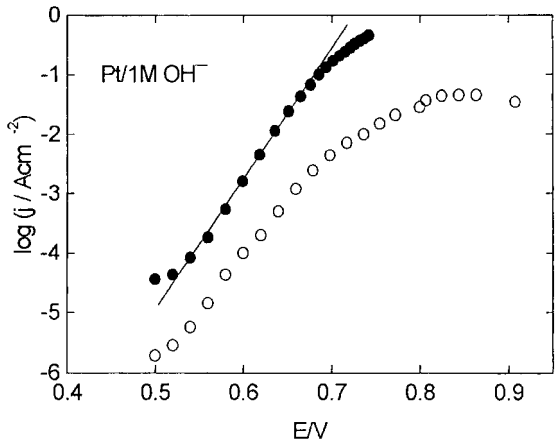

Fig. 6. Polarization plots for oxygen evolution in 1 M NaOH, 25 °C, corresponding to (●) electrodes I on Pt and (○) clean Pt.

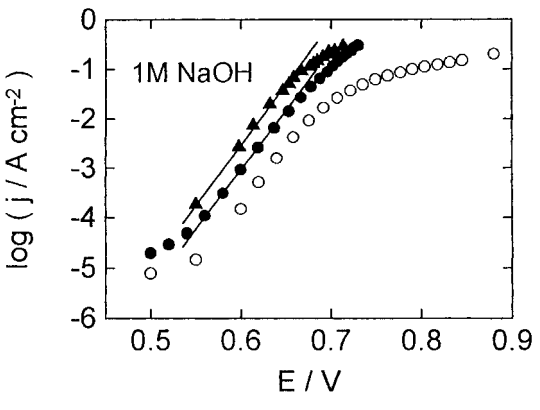

Fig. 8. Polarization plots for oxygen evolution in 1 M NaOH, 25 °C, corresponding to (●) electrodes I on Ni, (▲) electrodes II and (○) clean Ni.

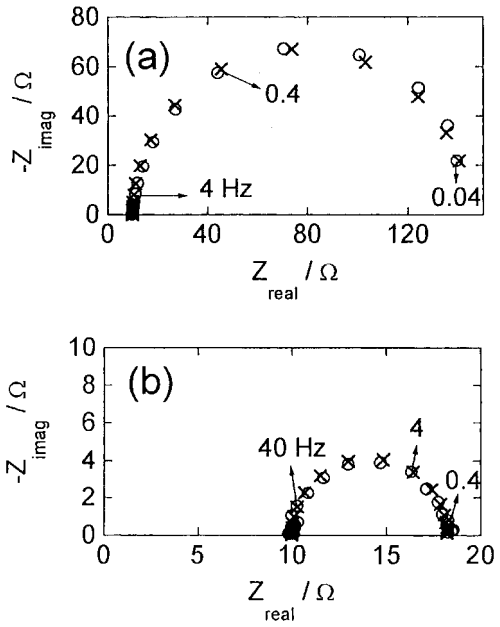

Fig. 9. Nyquist plots measured at $E = 0.6$ V (a) and $E = 0.7$ V (b), corresponding to electrodes I on Pt. 1 M NaOH, 25 °C. Key: (○) experiment, (×) simulated.

sponding to Fe substrate show a small additional capacitive contribution in the high frequency range, probably due to the underlying Fe-oxide passive film introducing another capacitive (C_{ox}) and resistive (R_{ox}) element. This impedance behaviour closely resembles impedance data previously reported for Co_3O_4 prepared by thermal decomposition on Ni and Ti substrates [17]. Accordingly, impedance data corresponding to electrodes I may be simulated in terms of the equivalent circuit of Fig. 11(a), where R_Ω corresponds to the electrolyte resistance, C_{dl} is the double layer capacitance associated with the Co-oxide/electrolyte interface, R_{ct}, C_{pc} and R_1 are potential dependent parameters related to the OER mechanism, C_{pc} denotes the pseudo-capacitance associated with the potential-dependent surface coverage of an adsorbed intermediate in the OER mechanism.

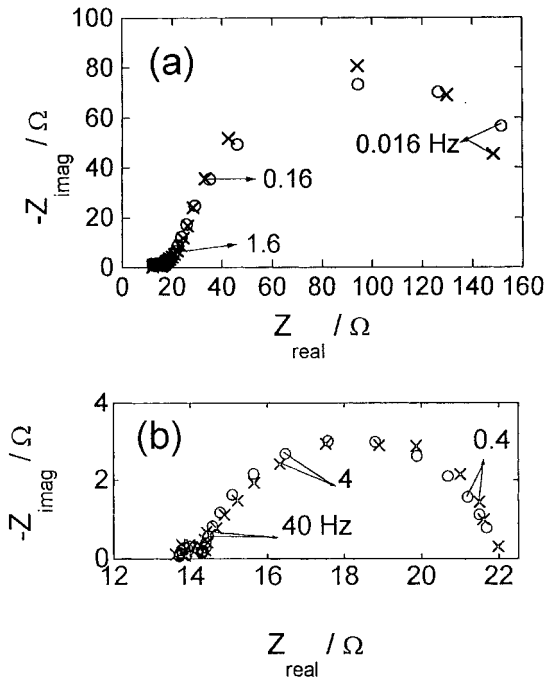

Fig. 10. Nyquist plots measured at $E = 0.6$ V (a) and $E = 0.7$ V (b), corresponding to electrodes I on Fe. 1 M NaOH, 25 °C. Key: (○) experiment, (×) simulated.

The impedance response of electrodes I on Ni and Pt substrates may be simulated by the simplified circuit on Fig. 11(b) as the contribution of the underlying oxide was not detected. An additional simplification is possible when $R_{ct} \ll R_1$, as shown in Fig. 11(b) being C_1 the linear combination of C_{dl} and C_{pc}, and R_1 the polarization resistance, equivalent to the impedance of the rate determining step (r.d.s.) when $f \to 0$. The parameters R_Ω, C_1 and R_1 included in Table 1 were calculated by a NLLS fit routine, in terms of the geometric area. The best-fit results (also shown in Figs 9 and 10) exhibit good agreement with the experimental data.

Experimental data corresponding to electrode I on Fe have been fitted in terms of the equivalent circuit in Fig. 11(c) and the best-fit parameters are included in Table 1.

In the case of electrodes II, the OER process dominates the impedance response of the system at smaller overpotentials than for electrodes I (Fig. 5). Nyquist plots corresponding to electrodes II, measured at $E = 0.6$ and 0.7 V are shown in Fig. 12. The less satisfactory signal-to-noise ratio observable in Fig. 12(b) is caused by the evolution of oxygen bub-

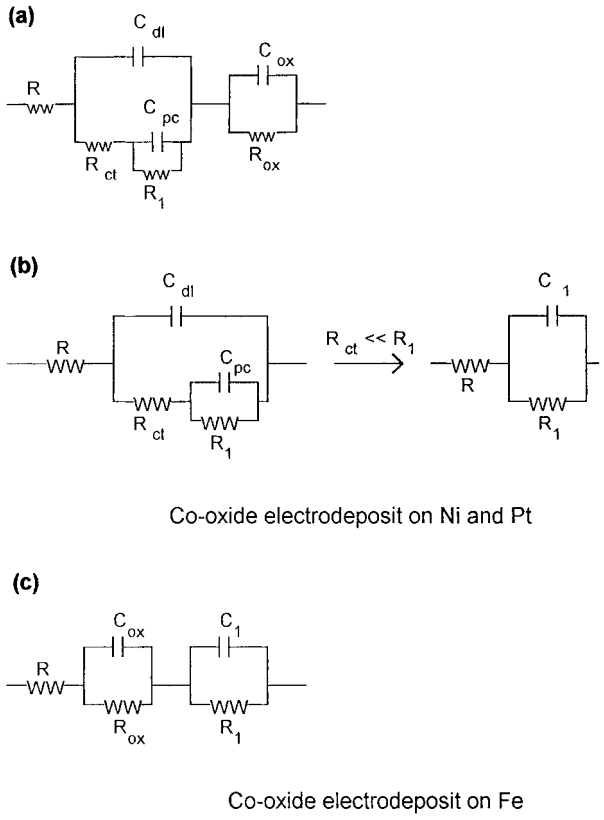

Fig. 11. Equivalent circuit used to fit the experimental impedance spectra of the electrochemical processes at Co-oxide films on different substrates.

Table 1. NLLS-fit parameters of the elements on equivalent circuits of Fig. 11

(a) Electrodes I

Co-oxide/Pt *Potential*/V	R_Ω/Ω cm^2	C_1/F cm^{-2}	R_1/Ω cm^2
0.60	1	5×10^{-2}	13.40
0.65	1	3.8×10^{-2}	1.60
0.70	1	2.55×10^{-2}	0.8
0.75	1	2×10^{-2}	0.41
0.80	1	1.5×10^{-2}	0.24

Co-oxide/Ni *Potential*/V	R_Ω/Ω cm^2	C_1/F cm^{-2}	R_1/Ω cm^2
0.60	1	3.6×10^{-1}	20
0.65	1	3.16×10^{-1}	2.28
0.70	1	2.9×10^{-1}	0.8
0.75	1	2.3×10^{-1}	0.38

Co-oxide/Fe *Potential*/V	R_Ω/ Ω cm^2	C_{ox}/ F cm^{-2}	R_{ox}/ Ω cm^2	C_1/ F cm^{-2}	R_1/ Ω cm^2
0.60	1	2×10^{-5}	0.2	2.5×10^{-1}	16.5
0.65	1	1.6×10^{-5}	0.3	2.1×10^{-1}	2.5
0.70	1	$\sim 5 \times 10^{-5}$	0.1	1.5×10^{-1}	0.77

(b) Electrodes II

Potential/V	R_Ω/Ω cm^2	C_1/F cm^{-2}	R_1/Ω cm^2
0.54	1	2.5×10^{-3}	455
0.60	1	3.28×10^{-3}	9.1
0.65	1	2.73×10^{-3}	1.34
0.70	1	2.61×10^{-3}	0.5
0.75	1	2.18×10^{-3}	0.32

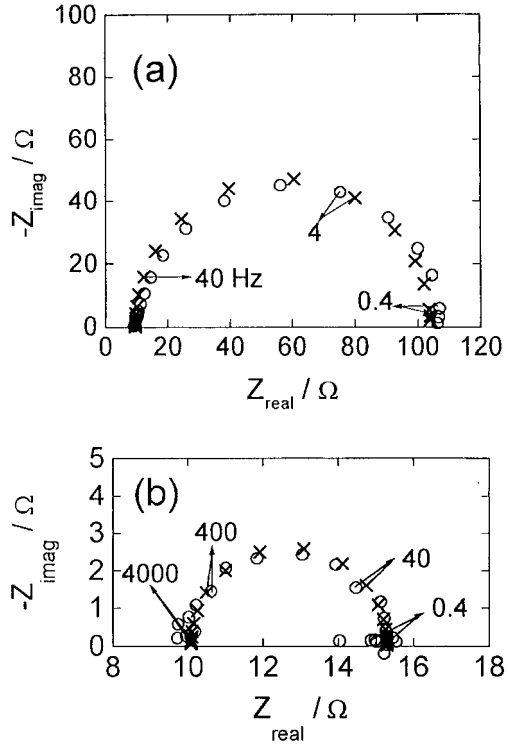

Fig. 12. Nyquist plots corresponding to electrodes II, measured at $E = 0.6$ V (a) and $E = 0.7$ V (b). 1 M NaOH, 25 °C. Key: (○) experiment, (×) simulated.

bles. Impedance data were fitted in terms of the equivalent circuit of Fig. 11(b); the parameters C_1 and R_1 determined by the fit routine are included in Table 1(b). The Tafel slope b_t calculated by: $b_t = 2.303\, R_1\, i$ (where i is the current density), was $b_t = 40$ mV dec^{-1} for $E < 0.7$ V. In accordance with steady state data, this value agrees with b_t calculated for electrodeposits I. The parameter C_1, associated with electrodeposits II, is two orders of magnitude smaller than for electrodeposits I on Ni substrate, probably on account of the smaller interfacial area. R_1 also has smaller values for higher current densities for the OER.

4. Discussion

Cobalt oxides prepared by potentiostatic electrodeposition, on different substrates (electrodes I), and potentiodynamic electrodeposition on Ni substrates (electrodes II), are probably cobaltites, having a stoichiometric composition close to Co_3O_4 for electrodes I and to $Ni_xCo_{3-x}O_4$ for electrodes II. In this case Co ions in the Co_3O_4 matrix are probably substituted by Ni ions leading to a nonhomogeneous distribution of Co and Ni ions in the lattice [3].

Voltammetric and EIS studies indicate that, before oxygen evolution, the surface of the Co electrodeposits is oxidized, probably to tetravalent oxidation states Co(IV) and Ni(IV) as already reported for cobaltite electrodes prepared by other techniques [9, 14, 17, 18].

From polarization and impedance measurements performed in the OER potential range, values for the Tafel slope, $b_t = 40$ mV dec^{-1}, were determined at low overpotentials. Both types of electrodeposits seem to provide similar mechanistic paths for the OER. Tafel slopes of 40 mV dec^{-1} were determined with Co_3O_4/RuO_2 supported on Ti and with $NiCo_2O_4$ [19, 20], although different values of b_T for spinel oxides, have been reported, depending on the preparation method, types of support and other experimental conditions. b_T values close to 40 mV dec^{-1} can be attributed to the second electron transfer step being rate determining [20]. Impedance spectra performed in a wide frequency range show only one capacitive contribution related to the OER process. This capacitive time constant is associated with the potential dependent surface concentration of only one intermediate state, probably OH or O adsorbed species.

Although further studies are needed, as for example the determination of the reaction order with respect to OH^-, we shall introduce a simplified mechanism for the OER on electrodes I and II. This reaction scheme is similar to the mechanism proposed by Conway and Liu [17] for Co_3O_4 on Ni and Ti substrates.

It has already been stated [17, 21] that oxygen is generally evolved at significant rates only when potentials corresponding to some higher oxidation state of the oxide are attained. In the present case surface oxidation can give rise to Co(IV) and NI(IV) surface states:

$$\mathrm{Co(III)_s} \Leftrightarrow \mathrm{Co(IV)_s} + \mathrm{e^-}$$
or
$$\mathrm{Ni(III)_s} \Leftrightarrow \mathrm{Ni(IV)_s} + \mathrm{e^-} \quad \text{(I)}$$

where $\mathrm{Co(III)_s}$, etc. denote atoms at the oxide surface.

Then, the OER can proceed through the following reaction:

$$\mathrm{Co(IV)_s} + \mathrm{OH^-} \Leftrightarrow \mathrm{Co(IV)(OH^-)_{ad}} \Leftrightarrow \mathrm{Co(III)(OH)_{ad}} \Leftrightarrow \mathrm{Co(IV)(OH)_{ad}} + \mathrm{e^-}$$

Ni(IV) species may participate in the same way as Co(IV).

This series of very reversible steps can be written as [6]

$$\mathrm{Co(IV)_s} + \mathrm{OH^-} \Leftrightarrow \mathrm{Co(IV)(OH)_{ad}} + \mathrm{e^-} \quad \text{(II)}$$

followed by

$$\mathrm{Co(IV)(OH)_{ad}} + \mathrm{OH^-} \rightarrow Co(\mathrm{IV})_s + 1/2\mathrm{O_2} + \mathrm{H_2O} + \mathrm{e^-} \quad \text{(r.d.s.)} \quad \text{(III)}$$

In process (III) the charge transfer r.d.s. is probably followed by other fast steps leading to oxygen evolution.

Considering step (III) as the r.d.s., and assuming Langmuir adsorption conditions, the reaction rate may be expressed by

$$v_{\mathrm{III}} = k_{\mathrm{III}} C_{\mathrm{OH^-}} \theta \exp\left(\frac{\beta FE}{RT}\right) \quad (1)$$

where θ is the surface concentration of the $\mathrm{Co(IV)(OH)_{ad}}$ intermediate.

Assuming low values of surface coverage and considering quasi-equilibrium conditions for process (II), θ may be evaluated by means of kinetic [6] or thermodynamic considerations:

$$\theta = k_{\mathrm{II}} C_{\mathrm{OH^-}} \exp\left(\frac{FE}{RT}\right) \quad (2)$$

and

$$v_{\mathrm{III}} = k(C_{\mathrm{OH^-}})^2 \exp\left(\frac{(1+\beta)FE}{RT}\right) \quad (3)$$

The mechanism represented by processes (II) and (III) may explain the value of $b_t = 40\,\mathrm{mV\,dec^{-1}}$, and the existence of only one capacitive contribution in the impedance spectra, associated with the potential dependence of the surface concentration of the $\mathrm{Co(IV)(OH)_{ad}}$ intermediate. It is interesting to note that this mechanism predicts a reaction order of 2.0 in accordance with experimental data presented in [6].

5. Conclusions

Cobaltoxides electrodeposited on Ni, Pt, Fe and vitreous C substrates, exhibit enhanced reactivity towards the OER, together with good chemical stability in alkaline solutions. Electrodes I, (co-oxides prepared by potentiostatic polarization), exhibit voltammetric profiles similar to Co_3O_4 spinel type oxides. Cyclic voltammograms corresponding to electrodes II, (co-oxides prepared by potentiodynamic electrodeposition on Ni substrates), are similar to $NiCo_2O_4$. The OER process appears to take place by similar mechanisms on both types of electrodeposits, although a better performance may be assigned to electrodes II.

Acknowledgements

This research project was financially supported by the Consejo Nacional de Investigaciones Científicas y Técnicas, the Comisión de Investigaciones Científicas de la Provincia de Buenos Aires, and The Fundación Antorchas.

References

[1] M. Hamdani, J. F. Koenig and P. Chartier, *J. Appl. Electrochem.* **18** (1988) 561.
[2] Y.-Sh. Lee. Ch.-Ch. Hu and T.-Ch. Wen, *J. Electrochem. Soc.* **143** (1994) 1218.
[3] M. R. Gennero de Chialvo and A. C. Chialvo, *Electrochimica Acta* **38** (1993) 2247.
[4] S. Trasatti, *ibid.* **29** (1984) 1503.
[5] S. G. Real, A. C. Elias, J. R. Vilche, C. A. Gervasi and A. Di Sarli, *ibid.* **38** (1993) 2029.
[6] R. N. Singh, J.-F. Koenig, G. Poillerat and P. Chartier, *J. Electrochem. Soc.* **137** (1990) 1408.
[7] F. A. Cotton and G. Wilkinson, *in* 'Advanced Inorganic Chemistry', (edited by F. A. Cotton and G. Wilkinson) J. Wiley & Sons, New York (1966), p. 897.
[8] L. C. Schumacher, I. B. Holzhueter, I. R. Hill and M. J. Dignam, *Electrochim. Acta* **35** (1990) 975.
[9] P. Nkeng, G. Poillerat, J. F. Koenig, P. Chartier, B. Lefez, J. Lopiteaux and M. Lenglet, *J. Electrochem. Soc.* **142** (1995) 1777.
[10] S. Maximovitch, *Electrochim. Acta* **41** (1996) 2761.
[11] E. B. Castro and J. R. Vilche, *ibid.* **38** (1993) 1567.
[12] C. Y. Cho, L. F. Lin and D. D. Macdonald, *J. Electrochem. Soc.* **129** (1982) 1874.
[13] E. B. Castro, *Electrochim. Acta* **39** (1994) 2117.
[14] R.-N. Singh, M. Hamdani, J.-F. Koenig, G. Poillerat, J. L. Gautier and P. Chartier, *J. Appl. Electrochem.* **20** (1990) 442.
[15] T. Ch. Wen and Ch.-Ch. Hu, *J. Electrochem. Soc.* **139** (1992) 2158.
[16] S. Jin, S. Ye, *Electrochim. Acta* **41** (1996) 827.
[17] B. E. Conway and T. C. Liu, *Ber. Bunsenges. Phys. Chem.* **91** (1987) 461.
[18] R. Boggio, A. Carugati and S. Trasatti. *J. Appl. Electrochem.* **17** (1987) 828.
[19] L. D. Burke and M. M. McCarthy, *J. Electrochem. Soc.* **135** (1988) 1175.
[20] G. Singh, M. M. Miles and S. Srinivasan, *in* 'Electrocatalysis on Nonmetallic Surfaces' (NBS Special Publication N°455) (edited by A. D. Franklin), US Government Printing Office, Washington, DC (1976), p. 289.
[21] A. C. C. Tseung and S. M. Jasem, *Electrochim. Acta* **22** (1976) 501.
[22] Y. W. D. Chen and R. N. Noufi, *J. Electrochem. Soc.* **131** (1984) 1447.